

# TITAN MONTGOLFIERE BALLOON ANALYSIS AND DESIGN USING COMPUTATIONAL FLUID DYNAMICS SIMULATIONS

Walter Dieudonne<sup>(1)</sup>, Yuri Feldman<sup>(2)</sup>, Jeffery L. Hall<sup>(3)</sup>, Tim Colonius<sup>(4)</sup>, Andre Vargas<sup>(5)</sup>, Jack A. Jones<sup>(6)</sup>, Kim Reh<sup>(7)</sup> and Julian Nott<sup>(8)</sup>

<sup>(1)</sup> *Research in Technologies for Innovation in Modeling the Environment, 6 Résidence Chataigniers, 09000 Vernajoul, France. Email: walter.dieudonne@rttime.fr*

<sup>(2)</sup> *California Institute of Technology, Mail Code 104-44, Pasadena, CA, USA, 91125 Email: yurifeld@caltech.edu*

<sup>(3)</sup> *Jet Propulsion Laboratory, California Institute of Technology, 4800 Oak Grove Dr., Mail Stop 82-105, Pasadena, CA., USA, 91109. Email: jlhall@mail.jpl.nasa.gov*

<sup>(4)</sup> *California Institute of Technology, Mail Code 104-44, Pasadena, CA, USA, 91125 Email: colonius@caltech.edu*

<sup>(5)</sup> *CNES Centre National d'Etudes Spatiales, 18, Av. Edouard. belin, 31401 Toulouse cedex 9, France. Email: Andre.Vargas@cnes.fr*

<sup>(6)</sup> *Jet Propulsion Laboratory, California Institute of Technology, 4800 Oak Grove Dr., Mail Stop 157-316, Pasadena, CA., USA, 91109. Email: jack.a.jones@jpl.nasa.gov*

<sup>(7)</sup> *Jet Propulsion Laboratory, California Institute of Technology, 4800 Oak Grove Dr., Mail Stop 321-625, Pasadena, CA., USA, 91109. Email: kreh@mail.jpl.nasa.gov*

<sup>(8)</sup> *Nott Technology LLC, 1482 East Valley Road, Santa Barbara, CA, USA 93108. Email: nott@nott.com*

## ABSTRACT

In this paper a multiple-layer heated balloon is considered for future Titan missions. We describe computational fluid dynamics (CFD) studies aimed at predicting the buoyancy for double-, triple-, and quadruple-walled balloons, and determining the sensitivity to the location of an external heat source. The buoyancy predictions from CFD show that the effective gap conductivity is higher than what is predicted by engineering correlations. Direct and large-eddy simulations (DNS/LES) are carried out for an idealized concentric spherical annulus with isothermal walls in order to investigate the source of the discrepancy and the resulting data is then used to design a new correlation. Results for multiple-layer balloons show the allowable scientific payload grows rapidly with increasing number of walls.

Next, the location of the heat source is analyzed, and we consider locations internal and external to the balloon. It is found that regardless of its location, an externally located heat source generates too much wasted heat and balloon performances is degraded substantially. A second design study deals with the external payload (gondola) and its effect on the balloon filling (blockage effects). It is found that even though important reductions in filling rates take place, it does not affect the overall descent rate, primarily due to the low gravity on Titan..

## 1. INTRODUCTION

In this paper various design issues are presented for a multiple-wall Montgolfiere balloon for a Titan

mission. A scientific payload within an external gondola hanging from the balloon has to fly at a constant ceiling altitude. The Titan balloon is powered with a RTG type heat source.

The buoyancy prediction for multiple walled balloon is first looked at with an emphasis onto the Nusselt to Rayleigh correlation that is used in engineering level studies. Configurations from two to four walled balloons are investigated and are compared one another to evaluate the achievable payload gains.

Using computational fluid dynamics, the location of the balloon heat source (RTG) used to maintain the system aloft is compared between a baseline internal location and varying external locations. This is done as having an externally placed heat source (for example on the scientific gondola) would provide an easier system integration. Finally, the location of the external scientific gondola is varied to make sure one is not facing with blockage effects that would prevent the balloon from properly inflating and filling during the injection phase.

## 2. BUOYANCY PREDICTION

This section summarizes the development of a computational fluid dynamic (CFD) model for accurate prediction of the Titan Montgolfiere buoyancy. Preliminary validation of the CFD model was provided by comparison with cryogenic tests of a small-scale balloon in the Titan Sky Simulator [1], and a more extensive validation was obtained from recent experiments at the same scale in the Wyle cryogenic facility [2]. The validated CFD model has since been used to model the full-scale cryogenic balloon.

Particular attention has been paid to evaluating the insulating effect associated with double- or even multiple-walled designs that are necessary to minimize the necessary heat input for a long duration flight on Titan. These CFD calculations reveal inaccuracies in engineering correlations for the effective conductivity of a spherical gap [2]. As such correlations are needed for system-level models, a detailed study of insulating gap was initiated.

In order to discern the source of discrepancy with correlations, simulations were conducted first for an idealized geometry that considers isothermal hot (inner) and cold (outer) spheres [3]. This setup eliminates additional effects associated with non-uniform surface temperatures of the real balloon which appear to be adequately captured in CFD. Both transitional and fully turbulent convection were considered and the computations were performed with the open source software openFoam [4].

Utilizing the modified heat transfer correlation for the narrow spherical gap [3] we also present analysis of a full scale multiple-walled balloon. The performance of multiple-walled balloon predicted by engineering correlations is compared with the corresponding CFD results and general conclusions with regards to optimal number of the gap sub layers are drawn.

## 2.1. Narrow shell analysis:

To characterize heat flux rate through the gap boundaries the functional dependence of Nusselt number  $Nu$  on Rayleigh number  $Ra$  is investigated.  $Nu$  and  $Ra$  are defined as:

$$Nu = \frac{1}{\pi D_o D_i} \oint \frac{\partial \theta}{\partial \hat{n}} dA, \quad Ra = \frac{g \beta}{\nu \alpha} \Delta T L^3 \quad (1)$$

where  $D_o, D_i, \theta, \hat{n}$  are non dimensional external diameter, internal diameter, temperature and normal vector respectively,  $g$  is the gravitational acceleration,  $\beta$  is the isobaric coefficient of thermal expansion,  $\nu$  is

the kinematic viscosity,  $\alpha$  is the thermal diffusivity,  $\Delta T$  is the temperature difference between cold and hot shell boundaries and  $L$  is the gap width. We used  $L, \Delta T, U = \sqrt{g \beta L \Delta T}, t = l/U, P = \rho U^2$  scales to normalize length, temperature, velocity, time and pressure respectively. Fig. 1 summarizes large eddy simulation (LES) results for  $Nu-Ra^*$  relationship obtained for the values  $\phi = 0.85, 0.90, 0.95$  and  $Ra^*$  up to  $2 \times 10^8$  with the superimposed direct numerical simulation (DNS) results obtained for the low  $Ra^*$  numbers. Here  $Ra^* = 2Ra \cdot L/D_i$  is a modified Rayleigh number introduced by Scanlan et al. [5] in an attempt to scale out the effect of different shell widths and  $\phi = D_i/D_o$  is internal to external diameter ratio. These values of  $Ra^*$  number cover the full range of gaps up to a 15 meter-diameter double-walled Titan Montgolfiere. Note an excellent agreement between the average  $Nu$  values predicted by both LES and DNS approaches for 5 different cases which verifies a correct resolving of the near wall temperature gradients by the LES model. We also verified that the same time-averaged value of  $Nu$  was obtained at both external and internal boundaries confirming accurate conservation of the heat flux. It is evident that both the DNS and LES approaches collapse fairly well on a power-law relation for  $Nu-Ra^*$  relationship but at the same time yield considerably higher slopes when compared to Scanlan et al. [5]. The higher slope implies an enhanced heat flux rate intrinsic to the narrow shells for even slightly super critical regimes. It is remarkable that about the same value of the  $Nu - Ra$  slope ( $Nu \sim Ra^{\approx 0.3}$ ) was also observed both numerically [7], [8] and experimentally [9] for turbulent natural convection inside differentially heated cavities. The reported simulations were performed up to moderate  $Ra < 10^{10}$  values of Rayleigh numbers, for which the thinnest conductive layers near the walls still exist and are not penetrated by the nearest small-scale turbulence flow structures. We would expect the same behavior for the narrow shell configuration, characterized by close to each other vertical and horizontal boundaries whose local curvature at the near equatorial and pole regions can be neglected.

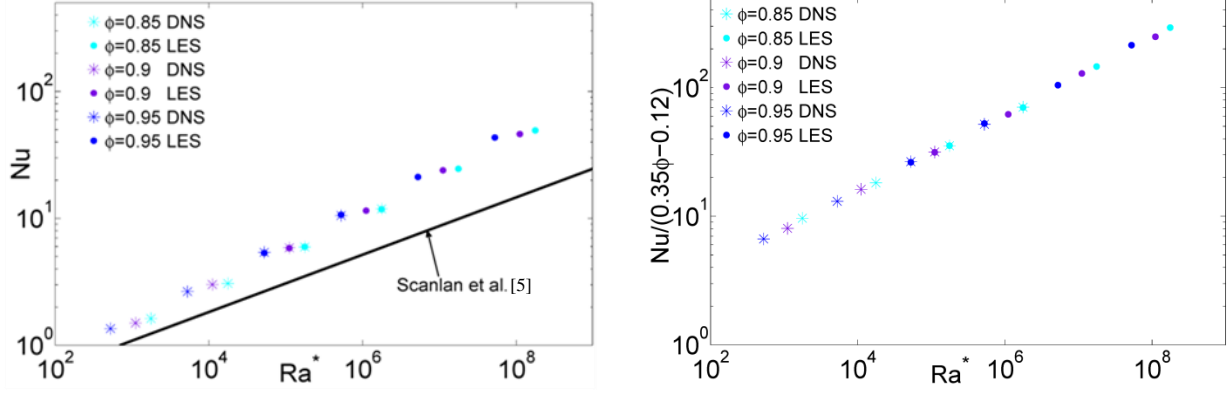


**Fig. 1: Details DNS and LES results for the  $Nu - Ra^*$  relationship: (a) three separate sets for  $\phi = 0.85, 0.90, 0.95$ ; (b) a single curve.**

As follows from the Fig. 1(a), the modified  $Ra^*$  in itself does not scale out the shell width effect for the narrow shells ( $0.85 \leq \phi \leq 0.95$ ) and three separate  $Nu - Ra^*$  curves for each  $\phi$  are observed. Noting the monotonic growth of the  $Ra^*$  coefficient with  $\phi$ , corresponding to the curve intercept, and a very slight variation of the  $Ra$  power ( $\approx 0.30$  up to a second decimal digit), we suggest a new scaling which would explicitly account for gap width:

$$Nu = (0.35\phi - 0.12)Ra^{*0.3}, \quad (2)$$

$$0.85 \leq \phi \leq 0.95, 10^3 \leq Ra^* \leq 10^8$$

The scaled results collapse on a single curve as shown in Fig. 1b. It should be noted that the suggested correlation was derived and numerically verified for  $Pr = 0.71$  and only the range  $Ra^*$  and  $\phi$  values given in Eq. 2. We would not recommend to apply it for extended range of  $\phi$  and  $Pr$  values without additional validation (numerical or experimental). At the same time the developed methodology and general observations regarding the free convection flow features intrinsic to narrow shells at a given range of  $Ra$  values are believed to be general and may be useful for the future research in this area.

## 2.2. Multiple-walled design:

Titan Montgolfiere design can be optimized by applying a multiple-walled concept, splitting up its insulating gap into a number of sub layers. In this case it is appropriate to focus on analysis of the balloon payload defined as a difference between the buoyancy

value and the balloon own weight. The later is based on a specific weight of the balloon's fabric (presently estimated conservatively at  $50 \text{ g/m}^2$ ) and the total area of the balloon walls. For multiple-walled balloon we distinguish between the global parameter  $\phi$ , previously defined as the ratio between the internal and external diameters, and the local parameter  $\phi_n$  calculated as the ratio between the diameters of two subsequent sub layers  $D_n$  and  $D_{n+1}$  respectively. To simplify the present analysis we assumed a constant value of  $\phi = 0.90$  and uniform width for all the gap sub layers.

Fig. 2 compares between the payloads (buoyancy less the fabric mass) obtained for the different balloon configurations as a function of heat input. The payload values marked by both dotted and solid lines were calculated by utilizing engineering heat transfer correlations determining heat flux rate through the balloon boundaries. The computation methodology is detailed in [1], and based on external [10], internal [11] and different gap ([5] for dotted and Eq. (2) for solid lines) engineering correlations defining relationships between the corresponding  $Nu$  and  $Ra$  numbers. As mentioned in [2] and verified in [3] it is the specific choice of gap correlation that makes a great difference (presently of more than 50%) between the predicted payload values. A good agreement is observed between the payloads predicted by engineering correlations with gap correlation proposed in Eq. (2) and those obtained by CFD calculations. The later were based on axis-symmetric geometry and Reynolds averaged Navier Stokes (RANS) turbulence modeling. At the same time the gap correlation of Scanlan et al. [5] considerably over-predicts the overall balloon buoyancy yielding about 2 times larger payloads for double- triple- and quadruple-walled balloons, respectively.

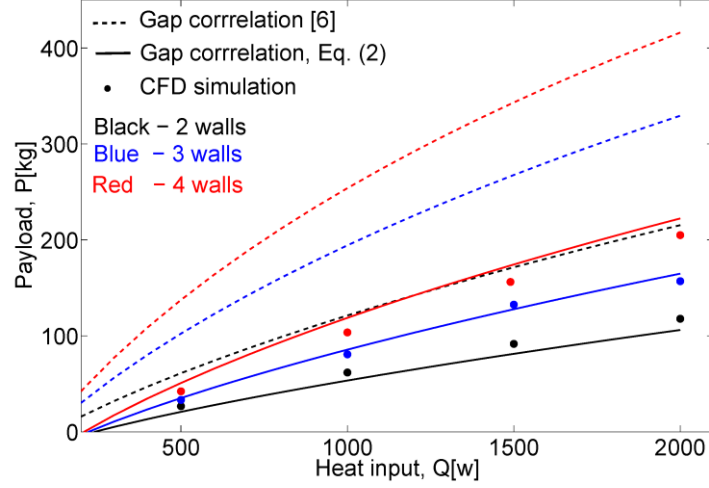


**Fig. 2: Comparison between the payloads predicted by engineering correlations and those simulated by CFD with RANS turbulence modeling.**

A good agreement between the numerically obtained payloads and those predicted by the system level approach, based on the modified gap correlation (2), motivated its further deployment for analysis of the balloons with varying diameters. The latter allows us to determine the minimal dimensions of the Titan Montgolfier operating with different heat inputs and sustaining a realistic scientific payload. Fig. 3 presents payloads predicted for the different balloon configurations with external diameters in the range of  $3m \leq D_o \leq 15m$ . It is remarkable that large size balloons ( $10m \leq D_o$ ) are characterized by close to linear growth of payload values with both external diameter and heat input values. This observation is valid for all the studied configurations (see Fig. 3).

According to the results predicted by engineering correlations the insulating properties of the balloon gap rapidly increase with increasing of the number of the balloon walls resulting in turn in the balloon's payload growth. The later, however, cannot continue indefinitely since the own weight of multi-walled balloon will eventually become high enough to obliterate the buoyancy gain while the payload will achieve its asymptotic value. It is also not recommended to apply the modified correlation for heat transfer analysis of multi-layer gaps characterized by the values of  $\phi_n \geq 0.95$ . This in turn determines the maximal number of internal walls, which with assumption of  $\phi = 0.9$  and uniform width for all the gap sub layers should not exceed the value of  $n=4$ .

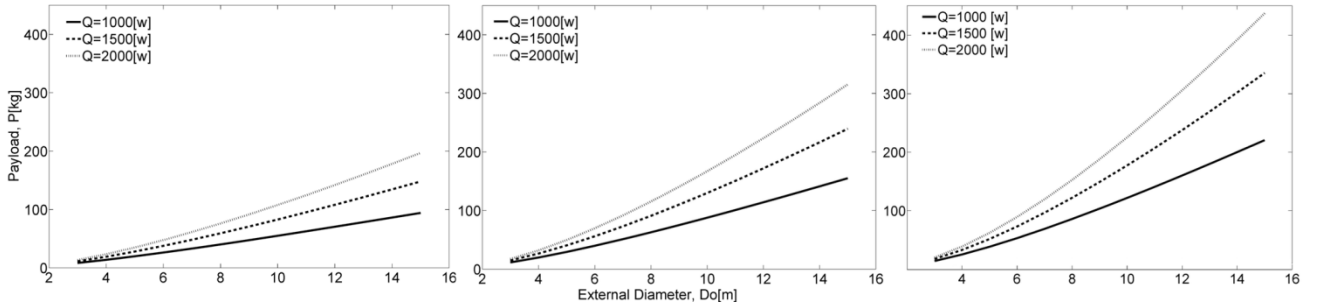


**Fig. 3: Payload versus external diameter of the Titan Montgolfier operating with three different heat inputs. The values predicted by engineering correlations utilizing the gap correlation proposed in [3]. From left to right: double-walled, triple-walled and quadruple walled balloon.**

### 3. TITAN BALLOON, RTG DESIGN

Compared to the standard double wall balloon design with an internal RTG, it is proposed to investigate an alternative design in which the internal heater is placed outside, on top of a gondola. The balloon performances in terms of lifting mass are investigated.

The baseline case is the standard configuration: internal RTG and a simple external gondola located 2[m] below the inlet. The other configurations deal with an external RTG sitting on top of the gondola; 3 gondola locations are considered: 2, 3 and 4[m] below the balloon inlet.

#### 3.1. Design specifications and flow conditions

Previous work has extensively studied the RTG location effect and power within the balloon. One conclusion was: the RTG located the lowest provides the highest buoyancy as the internal flow is the most homogeneous and the warmest.

One proposal now studied is to have the RTG placed outside the balloon; factually it sits on top of the science gondola.

In Fig. 4 the gondola is schematised, it is 1.60[m] wide and 0.46[m] high. The Titan double wall balloon set-up is: 10m diameter, 20 cm double wall gap and 1.00[m] entry diameter.

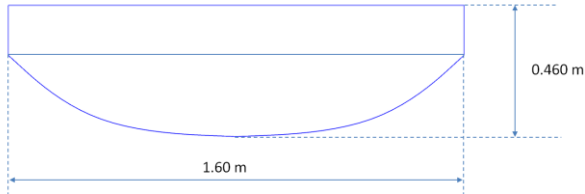


**Fig. 4: External science gondola dimensions.**

A RTG placed outside the balloon on top of the gondola would provide a simpler integration and a safer balloon deployment. From a fluid and thermal view point, one may anticipate that this external RTG design choice may lead to poorer performances (compared to the internal RTG) as some heat will be lost to the ambient atmosphere instead of the balloon internal flow.

Three gondola locations are considered: 2, 3, 4 [m] below the balloon inlet. It is decided not to use 1m as obviously blockage effects will become too important during the descent. A view of the configurations is showed in Fig. 5.

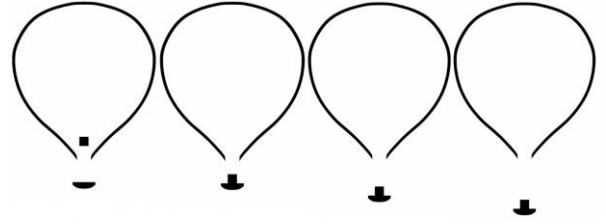


**Fig. 5: Geometries for the different design configurations; from left to right: baseline, high, middle, low gondola.**

#### 3.2. Buoyant mass results

From the CFD, we compare the baseline case (standard design) to the other options. The results for the buoyant mass  $B$  are presented in Table 1 and plotted in Fig. 6.

Case	Gondola distance [m]	Buoyant mass [kg]
Lowest gondola	-4	37.80
Middle gondola	-3	66.93
Highest gondola	-2	105.82
Baseline case with internal RTG	-2	254.17

**Table 1: Buoyant mass in [kg] for the baseline case and the external RTG cases**

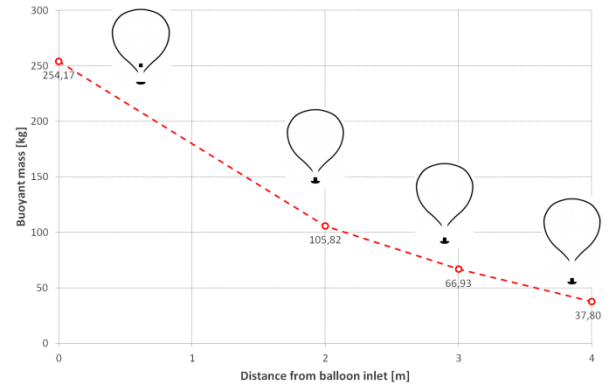


**Fig. 6: Buoyant mass in [kg] for the baseline case and the external RTG cases.**

The baseline results for the internal RTG are showed in Fig. 7. One sees a warm temperature field and a recirculatory flow that stays within the balloon. Thermal losses are only taking place through the envelope skins.

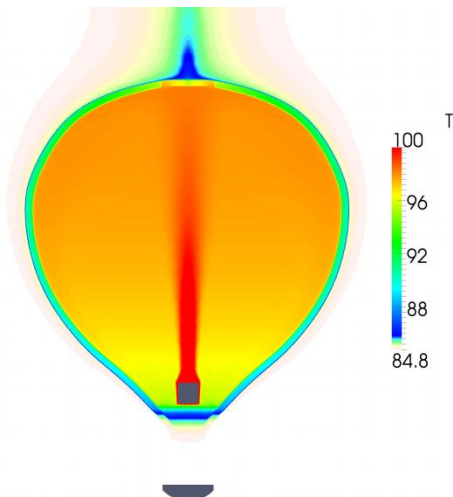


**Fig. 7: Baseline case (internal RTG), thermal field.**

Taking the case of the lowest gondola (4m below the inlet), the thermal field is showed in Fig. 8. One sees that the warm flow (flame like) is mostly concentrated between the gondola and the balloon inlet; the thermal plume within the balloon is very weak and the internal flow is cool. Streamlines show the cold external flow feeding the RTG. The velocity field (not showed) indicates weak balloon internal flow dynamics.

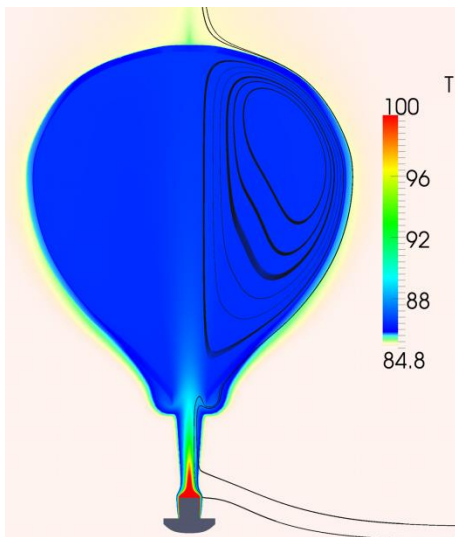


**Fig. 8: External RTG on the gondola, thermal field.**

To understand the reasons for the poor balloon performances in terms of lifting mass, one concentrates on the flow between the gondola and inlet. In Fig. 9 the thermal field is plotted together with the flow streamlines. There are 3 effects playing against performances:

- the RTG is fed with cold flow: the RTG warms up the external atmosphere instead of warming up the internal flow.
- the RTG plume flow presents spillage at the inlet: not all the warm flow goes inside the balloon and some warm flow is diverted outside the balloon.
- warm internal flow within the envelope is ejected outside because we are feeding the internal flow with external gas and the only mass exchange balloon is at the inlet. This flow ejection is partly responsible for the flow spillage.

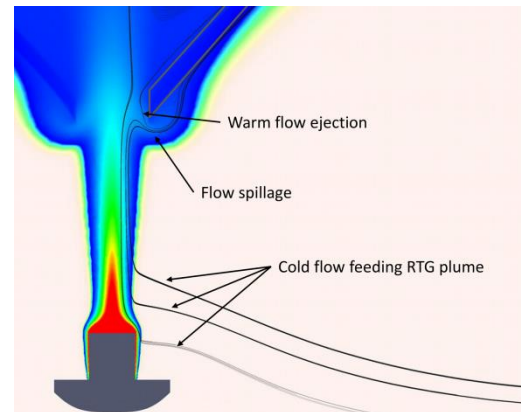


**Fig. 9: Details of energy losses when having an external RTG.**

A visual indicator for the balloon performances is the internal thermal field. Fig. 10 compares the baseline case (internal RTG) together with external RTG cases (-4, -3, -2m). One clearly sees the dramatic buoyant mass performance losses due to having an external RTG.

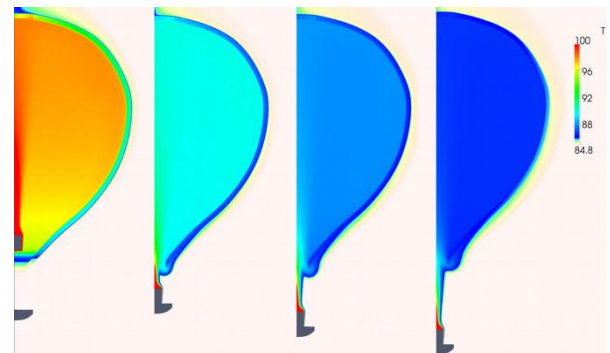


**Fig. 10: From left to right, buoyant mass visual representation through the thermal fields comparing the baseline case with the external RTG's (-2, -3, -4m).**

Performances for the ceiling conditions degrade tremendously because of combined fluid and thermal effects. This design must be avoided and it is important to keep the RTG heater within the balloon.

#### 4. DEPLOYMENT PHASE, TITAN

During the deployment phase, the balloon inner pressure is used to push away the balloon walls. Within the balloon pressure levels remain moderate and the flow enters freely.

Several cases with varying gondola distance are considered for the Titan initial deployment at 40km altitude. Three results are presented in Fig. 11 with a 1.6m gondola at 6, 4 and 2m below the 1m diameter inlet. It is seen that the gondola wake interacts with the inlet with varying degrees of importance.

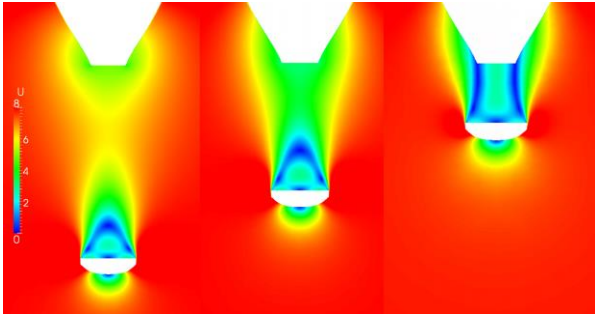


**Fig. 11: Gondola wake interaction with balloon inlet for Titan deployment at 40km for three configurations (6, 4, 2m gondola distance).**

Eventually, one wants to evaluate the mass flow rate at the balloon inlet as a function of the external gondola set-up. The mass flow ingestion rate relates to the deployment efficiency. In the end, one wants for each design, the overall balloon trajectory.

The 10m diameter double wall balloon with a 1m inlet and a 20cm gap width is used. Several vertical gondola locations are selected: from 2 to 6m below the inlet; additionally, a baseline case with no gondola is also carried out. It gives the inlet efficiency only taking into account viscous effects (the flow is assumed incompressible at speeds of 8 m/s). Flow conditions correspond to the maximum descent velocity at high altitude:  $P_\infty=98550$  [Pa],  $\rho_\infty=4.2733$  [kg/m<sup>3</sup>],  $T_\infty=77.7$  [K] and  $U_\infty=8$  [m/s].

The mass flow rate is evaluated for several gondola locations and compared to the baseline case (no gondola); the values are given in Table 2.

Gondola distance [m]	2	3	5	6	none baseline
Mass flow rate [kg/s]	5,60	5,77	13,59	15,26	20,55
Efficiency	27	28	66	76	100 %

**Table 2: Mass flow rate at the balloon inlet as a function of gondola distance from the inlet compared to the baseline case (no gondola). Ideal rate for inviscid flow = 26.85 [kg/s].**

Due to its wake, a gondola close to the balloon reduces the inlet efficiency and thus the balloon inflation rate will be reduced.

It is important to evaluate the balloon filling rate with respect to the balloon deployment and the balloon overall altitude profile. The baseline case is the Titan mission with the 200 kg payload, the 1740W RTG and no gondola. An efficiency factor is applied to the ingested mass flow to simulate perturbations due to the gondola wake (75, 50 and 25%).

Balloon filling rates are plotted in Fig. 12. It is seen that the time needed for the full inflation varies largely and is near 1 hour for the worst case corresponding to a gondola very close to the inlet.

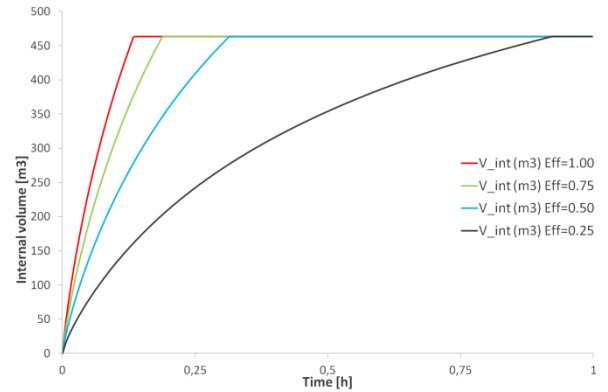


**Fig. 12: balloon internal volume as a function of time during the deployment phase; an efficiency factor (Eff) is applied on the ingested mass flow to reproduce gondola wake perturbations.**

The overall trajectory comparison for the baseline case and the less efficient inlet (25%) is presented in Fig. 13. It is seen that the inflation process has very little effect on the overall altitude process and that the ceiling altitude is not altered, even for strongly perturbed inlet inflation. This is a positive result as the system is robust to balloon inlet perturbations. This result can be explained by the very long descent time due to the low gravity. Factually, Titan conditions are more favorable than Earth conditions because of weak dynamics in a low gravity environment.

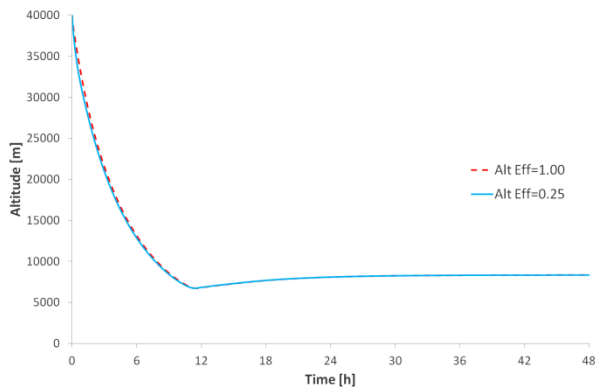


**Fig. 13: Altitude history plot for the Titan TSSM case comparing a regular balloon inlet with a poorly efficient (25%) inlet mass flow ingestion due to the gondola wake interactions.**

The external gondola creates a wake flow during the initial phase that perturbs the mass flow ingestion at the balloon inlet. The inflation process is substantially slowed down (up to 1 hour for full inflation). However, for the overall high altitude injection to ceiling altitude process, there is very little effects on the trajectory history. This is an important result that also indicates that the design is robust with respect to degradation in the balloon deployment.

## 5. CONCLUSIONS

In this study, three design issues have been investigated. The heat source location has been changed from its initial internal location (within the balloon) to several external locations. An externally located heat source must be avoided as the balloon performances (i.e. the allowable payload) is severely reduced. The scientific gondola has been placed at varying distances from the balloon inlet mouth. Even though strong wake flow from the gondola perturbs the balloon filling mass flow rate, it only has an overall weak influence on the injection to ceiling trajectory. Finally, an updated engineering correlation has been derived to provide the Nusselt values as a function of Rayleigh and gap geometry. CFD as well as engineering studies have demonstrated that the use of multiple layer (up to 4) is beneficial for the balloon performances even as skin mass is added as it increases the insulation in a sufficient manner.

## 6. REFERENCES

- [1]. A. Samanta, D. Appelö, T. Colonius, J. Hall, and J. Nott, Computational Modeling and Experiments of Natural Convection for a Titan Montgolfiere, *AIAA Journal*, 48(5):1007-1016, 2010
- [2] Yu. Feldman, T. Colonius, M. Pauken, J. Hall, J. Jones, Simulation and Cryogenic Experiments of Natural Convection for the Titan Montgolfiere, *AIAA Journal*, 50(11):2483-2491, 2012.
- [3] Yu. Feldman, T. Colonius, On a transitional and turbulent natural convection in spherical shells, submitted to *International Journal of Heat and Mass Transfer*.
- [4] H. Weller, G. Tabor, H. Jasak, C. Fureby, A tensorial approach to computational continuum mechanics using object-oriented techniques, *Computers in Physics* 12:620-631, 1998.
- [5] J. Scanlan, E. Bishop, R. Powe, Natural convection heat transfer between concentric spheres, *Int. J. Heat Mass Transfer* 13:1857-1872, 1970.
- [6] G. Raithby, K. Hollands, A general method of obtaining approximate solutions to laminar and turbulent free convection problems, *Advances Heat Transfer* 11:265-315, 1975.
- [7] N. Markatos, K. Pericleous, Laminar and turbulent natural convection in an enclosed cavity, *Int. J. Heat Mass Transfer* 27:755-772, 1984.
- [8] J. Xaman, G. Alvarez, L. Lira, C. Estrada, Numerical study of heat transfer by laminar and turbulent natural convection in tall cavities of facade elements, *Energy and Buildings* 37:787-794, 2005.
- [9] W. H. Leong, K. G. T. Hollands, A. P. Brunger, Experimental Nusselt numbers for a cubical-cavity benchmark problem in natural convection, *Int. J. Heat Mass Transfer* 42:1979-1989, 1999.
- [10] A. Campo, Correlation Equation for Laminar and Turbulent Natural-Convection from Spheres, *Wärme- und Stoffübertragung*, 13: 93-96, 1980.
- [11] L. A. Carlson, and W. J. Horn, New Thermal and Trajectory Model for High-Altitude Balloons, *Journal of Aircraft*, 20:500-507, 1983.